



1 **How well do operational Numerical Weather Prediction configurations represent**
2 **hydrology?**

3
4 Ervin Zsoter, European Centre for Medium-Range Weather Forecasts, Reading, UK;
5 Department of Geography and Environmental Science, University of Reading, Reading, UK
6 Current address: European Centre for Medium-Range Weather Forecasts, Shinfield Park,
7 Reading, RG2 9AX, UK

8
9 Hannah Cloke, Department of Geography and Environmental Science, University of
10 Reading, Reading, UK; Department of Meteorology, University of Reading, Reading UK;
11 Department of Earth Sciences, Uppsala University, Uppsala, Sweden and Centre of Natural
12 Hazards and Disaster Science, CNDS, Uppsala, Sweden

13
14 Elisabeth Stephens, Department of Geography and Environmental Science, University of
15 Reading, UK

16
17 Patricia de Rosnay, European Centre for Medium-Range Weather Forecasts, Reading, UK

18
19 Joaquin Muñoz-Sabater, European Centre for Medium-Range Weather Forecasts, Reading,
20 UK

21
22 Christel Prudhomme, European Centre for Medium-Range Weather Forecasts, Reading, UK

23
24 Florian Pappenberger, European Centre for Medium-Range Weather Forecasts, Reading, UK
25 and College of Hydrology and Water Resources, Hohai University, Nanjing, China

Early Online Release: This preliminary version has been accepted for publication in *Journal of Hydrometeorology*, may be fully cited, and has been assigned DOI 10.1175/JHM-D-18-0086.1. The final typeset copyedited article will replace the EOR at the above DOI when it is published.

26

27 Corresponding author: E. Zsoter, European Centre for Medium-Range Weather Forecasts,

28 Shinfield Park, Reading, RG2 9AX, UK (ervin.zsoter@ecmwf.int)

29 **Abstract**

30 Land surface models (LSMs) have traditionally been designed to focus on providing lower
31 boundary conditions to the atmosphere with less focus on hydrological processes. State of the
32 art application of LSMs include land data assimilation system (LDAS) which incorporates
33 available land surface observations to provide an improved realism of surface conditions.
34 While improved representations of the surface variables (such as soil moisture and snow
35 depth) make LDAS an essential component of any Numerical Weather Prediction (NWP)
36 system, the related increments remove or add water, potentially having a negative impact on
37 the simulated hydrological cycle by opening the water budget.

38

39 This paper focuses on evaluating how well global NWP configurations are able to support
40 hydrological applications, in addition to the traditional weather forecasting. River discharge
41 simulations from two climatological reanalyses are compared: one ‘online’ set which
42 includes land-atmosphere coupling and LDAS with an open water budget, and also an
43 ‘offline’ set with a closed water budget and no LDAS.

44

45 It was found that while the online version of the model largely improves temperature and
46 snow depth conditions, it caused poorer representation of peak river flow, particularly in
47 snowmelt-dominated areas in the high latitudes. Without addressing such issues there will
48 never be confidence in using LSMs for hydrological forecasting applications across the
49 globe. This type of analysis should be used to diagnose where improvements need to be
50 made; considering the whole Earth System in the data assimilation and coupling
51 developments is critical for moving towards the goal of holistic Earth System approaches.

52

53 **1 Introduction**

54 Land surface models (LSMs) have traditionally been designed to focus on providing lower
55 boundary conditions to the atmosphere by describing the vertical fluxes of energy and water
56 between the land surface and the atmosphere, with less focus on predicting runoff
57 (Mengelkamp et al. 2001). LSMs therefore maximise the quality of the atmospheric forecast,
58 but do not necessarily bring the same benefits in the representation of the hydrological cycle
59 (Kauffeldt et al. 2015).

60

61 There is a wide literature on assessing the hydrological capabilities of LSMs and describing
62 various improvements in the modelling of the hydrological cycle (e.g. Balsamo et al. 2009;
63 Wang et al. 2016; Blyth et al. 2011; Wu et al. 2014). However, there are significant
64 limitations in the representation of hydrological fluxes and storages in LSMs, largely due to
65 the large-scale focus of LSM applications, which has led to the neglect of some important
66 processes for runoff generation (Overgaard et al. 2006; Le Vine et al. 2016), including
67 inadequate snowmelt processes (Dutra et al. 2012, Zaitchik and Rodell 2009).

68

69 Data assimilation is an essential part of any Numerical Weather Prediction (NWP) system
70 (Rabier 2005). It is designed to provide initial conditions for the Earth System by updating
71 the model in all of the components: atmosphere, land, ocean and sea ice. State of the art NWP
72 configurations, such as used at the European Centre for Medium-Range Weather Forecasts
73 (ECMWF), include both an LSM and a land data assimilation system (LDAS). The objective
74 of the data assimilation in this context is to combine the land surface model state with the
75 available land surface observations to initialise the land surface model prognostic variables of
76 the forecasting system (Bélair et al. 2003). The current ECMWF LDAS analyses soil
77 moisture, soil temperature, snow mass, density and temperature (de Rosnay et al. 2014). Land

78 data assimilation was shown to contribute significantly to more skilful atmospheric forecasts,
79 with the soil moisture data assimilation also proven essential in countering a positive
80 precipitation/evapotranspiration feedback which can cause large positive precipitation biases
81 (e.g. de Rosnay et al. 2013; Drusch et al. 2007, Beljaars et al. 1996).

82

83 While the improved surface conditions make LDAS an essential component of the ECMWF
84 NWP system, by design the related increments remove or add water which can potentially
85 have a negative impact on the representation of the hydrological cycle by opening the water
86 budget (Zaitchik and Rodell 2009; Arsenault et al. 2013; Andreadis and Lettenmaier, 2006;
87 De Lannoy et al. 2012; Pan and Wood, 2006). On the contrary, in a system without LDAS
88 and coupling, the errors resulting from atmospheric forcing insufficiencies and imperfect land
89 surface process representations are not corrected by the assimilation of land surface
90 observations.

91

92 As an ideal configuration, an Earth System model should always maintain a closed water
93 budget, where the amount of water in the system remains the same. By opening the water
94 budget, river discharge biases could emerge in situations where the LSM has energy balance
95 bias that is not corrected by the assimilation but only by accurate precipitation and snow
96 accumulation forcing. For example, if the snow in the LSM is melting too slowly, this forces
97 the LDAS to remove water (through snow) artificially to correct for the excessive amount of
98 snow on the surface. If the water that is removed with the snow (and thus could not melt) is
99 not retained within the Earth System that could lead to soil water deficit downstream,
100 potentially causing an incorrect rate of river discharge. In such cases, LDAS could lead to
101 replace incorrect snowmelt timing issue with incorrect snowmelt runoff amount.

102

103 Thus, an open water budget could cause problems for associated hydrological forecasting
104 applications, which uses runoff calculated from LSMs with LDAS, such as the Global Flood
105 Awareness System (GloFAS; Alfieri et al. 2013). As global hydrological modelling is
106 increasingly possible with the improved realism that the state-of-the-art LSMs can nowadays
107 offer (Overgaard et al. 2006), it is important to investigate how an LSM with LDAS can
108 support the combined task of traditional weather forecasting and hydrology at the same time.
109 This investigation was undertaken with this dual focus in mind, by analysing the hydrological
110 cycle and the open water budget issues that can help the Earth System model developments
111 with highlighting areas where the coupled system with LDAS does not yet work effectively
112 for flood simulations.

113

114 In order to understand how well an NWP configuration with LSM and LDAS represents
115 hydrology, and in particular to interpret the influence of the LDAS on hydrological
116 simulations from LSMs, in this paper river discharge simulations from two climatological
117 reanalyses of GloFAS are compared: one operational set which includes land-atmosphere
118 coupling and LDAS with an open water budget, and also an ‘offline’ set with a closed water
119 budget and no LDAS. From these two datasets, a range of hydrological and atmospheric
120 variables will be analysed globally.

121

122 **2 System Description, datasets and methods**

123 Two hydrological experiments, ONLINE (run in operational mode with active land-
124 atmosphere coupling and LDAS) and OFFLINE (run in offline mode without coupling and
125 LDAS) provide time series of various surface variables (e.g. 2-metre temperature, snow depth
126 and runoff), and also discharge after routing the runoff. Figure 1 highlights the schematic of
127 ONLINE and OFFLINE with the main characteristics, components and data periods. In this

128 section the two experiments with the model and data aspects, and the data analysis methods
129 will be described in detail.

130

131 **2.1 Land surface model HTESSEL**

132 The hydrological component of the analysed data sets is based on the HTESSEL land surface
133 model (The Hydrology-Tiled ECMWF Scheme for Surface Exchange over Land; Balsamo et
134 al. 2009; Balsamo et al. 2011). HTESSEL is part of the ECMWF NWP system and used in
135 coupled land-atmosphere mode on time ranges from short-range to seasonal forecasts. It
136 includes a snow parameterisation based on a single-layer snow pack model (Dutra et al.,
137 2010). The soil vertical diffusion solves the Richards equation using a four-layer vertical
138 discretisation with layer depths at 7 cm, 28 cm, 100 cm and 289 cm (Balsamo et al. 2009).
139 HTESSEL provides boundary conditions for the atmosphere (heat, moisture, and momentum)
140 by simulating water and energy budgets on the surface and through the soil, snowpack and
141 vegetation interception. HTESSEL generates surface (fast) and subsurface (slow) runoff
142 components at each grid point (Balsamo et al. 2009). Surface runoff depends on the standard
143 deviation of the orography, soil texture and soil moisture, while subsurface runoff is
144 determined by the soil water percolation.

145

146 **2.2 Land data assimilation**

147 The ECMWF LDAS is part of the ECMWF Integrated Forecasting System (IFS). It is
148 coupled to the atmospheric four-dimensional variational (4-D-Var) data assimilation scheme
149 (Rabier et al. 2000), both using a 12-hour assimilation window. The upper air and land
150 surface analyses are running separately and used to initialise a coupled land-atmosphere
151 short-term forecast, which provides the background for the next data assimilation window.
152 The land data assimilation relies on advanced methods to optimally combine in situ and

153 satellite observations with model background information. A schematic diagram of the
154 ECMWF LDAS is provided in Figure 2.
155

156 Initial implementations of the ECMWF LDAS relied on simple assimilation methods for
157 snow and soil moisture analyses (Drusch et al. 2004, Mahfouf et al. 2000), with air
158 temperature and humidity measurements being the main input for the soil moisture analysis
159 (Mahfouf et al. 2000, Drusch et al. 2007). The system has evolved in the past decade to use a
160 more physically based approach and to combine satellite and in situ data in the soil analysis
161 (de Rosnay et al. 2014, de Rosnay et al. 2013, Albergel et al. 2012).
162

163 In the current LDAS, a simplified Extended Kalman Filter (SEKF) is used to analyse soil
164 moisture. The approach combines analysed 2-metre air temperature and humidity with
165 satellite measurements from the ASCAT (Advanced Scatterometer) sensor on board of
166 MetOp, as described in de Rosnay et al. (2013) and Albergel et al (2012). For snow, a two-
167 dimensional optimal interpolation (OI) is used to analyse snow mass and snow density
168 following the method described in Brasnett et al. (1999). In situ snow depth observations,
169 available on the SYNOP network are used along with the 4km resolution snow cover product
170 from the NOAA/NESDIS (National Environmental Satellite, Data, and Information Service)
171 Interactive Multi-sensor Snow and Ice Mapping System (IMS) product (Helfrich et al. 2007).
172

173 Even though it provides significant improvements to the atmospheric forecasts and
174 independent situ snow depth measurements (de Rosnay et al. 2015), the current ECMWF
175 snow data assimilation follows a relatively basic method. Operational NWP configurations
176 generally rely on simple approaches, compared to research environment, that are based on
177 more sophisticated snow assimilation methods using in situ and remotely sensed observations

178 (e.g. Helmert et al. 2018; De Lannoy et al. 2012; Pan and Wood 2006; Slater and Clark
179 2006).

180
181 The ECMWF LDAS and its performance is presented and discussed in de Rosnay et al.
182 (2014), and de Rosnay et al. (2015). A full description of the technical implementation is
183 provided in the IFS documentation ([https://www.ecmwf.int/en/forecasts/documentation-and-](https://www.ecmwf.int/en/forecasts/documentation-and-support/changes-ecmwf-model/ifs-documentation)
184 [support/changes-ecmwf-model/ifs-documentation](https://www.ecmwf.int/en/forecasts/documentation-and-support/changes-ecmwf-model/ifs-documentation)). The system used for this study is that
185 used for the production of ERA5 (section 2.6), with IFS cycle 41r2 at a resolution of ~31 km.

186

187 **2.3 CaMa-Flood river-routing**

188 The Catchment-based Macro-scale Floodplain model (CaMa-Flood; Yamazaki et al. 2011)
189 was applied in this study to simulate the hydrodynamics and produce river discharge from the
190 HTESSEL runoff outputs. CaMa-Flood is a distributed global river-routing model which uses
191 a river network map and routes runoff to oceans or inland seas. The CaMa-Flood model was
192 chosen for the routing component as it had already been used in several similar climatological
193 research experiments such as Emerton et al. (2017).

194

195 **2.4 GloFAS**

196 GloFAS is one of the few global scale flood forecasting systems that currently exist (Emerton
197 et al. 2016). It is part of the Copernicus Emergency Management Service (CEMS), developed
198 by the Joint Research Centre of the European Commission (JRC) and ECMWF. The
199 HTESSEL runoff output is coupled to the Lisflood hydrological model over a global river
200 network to produce river discharge with a forecast horizon of 30 days across a global river
201 network at 0.1 degree resolution (van der Knijff et al. 2010; Alfieri et al. 2013). As part of the
202 GloFAS configuration, the real-time river discharge forecasts are compared with

203 climatological simulations (called reanalysis) to detect the likelihood of high flow situations.
204 These real-time and climatological datasets also present a unique opportunity for
205 experimental analysis (Emerton et al. 2017; Stephens et al. 2015).

206

207 **2.5 Offline land surface modelling**

208 The current GloFAS operational set-up uses a climatology based on the ERA-Interim/Land
209 reanalysis of ECMWF (Balsamo et al., 2015). ERA-Interim/Land is an improved version of
210 the ERA-Interim reanalysis (Dee et al. 2011) produced with an improved version of
211 HTESSEL, run offline, using a rescaling of monthly precipitation totals with GPCP v2.2
212 (Huffman et al. 2009; Balsamo et al. 2010). “Offline” HTESSEL simulations, such as the
213 OFFLINE experiment in this study, are uncoupled from the atmosphere, without the LDAS
214 and forced with near-surface meteorological input data such as temperature, specific
215 humidity, wind speed, surface pressure, radiative fluxes and water fluxes. Offline land
216 surface only simulations are an affordable way of achieving land surface improvements and
217 this offline research methodology has been used in numerous studies with HTESSEL in the
218 last few decades (e.g. Agusti-Panareda et al. 2010; Dutra et al. 2010; Dutra et al. 2011;
219 Haddeland et al. 2011).

220

221 **2.6 ERA5 reanalysis**

222 The 5th generation global climate reanalysis (succeeding ERA-Interim) at ECMWF is ERA5
223 (Hersbach and Dee 2016). ERA5 is a key contribution to the EU-funded Copernicus Climate
224 Change Service (C3S). ERA5 will cover the period 1950-present and is in production with
225 2008-2017 already officially released. The release of the remaining period is foreseen by end
226 of 2018. ERA5 will then continue running in (non-quality assured mode) near-real time with
227 only a few days delay. The data is open access and free to download for all uses

228 (<https://climate.copernicus.eu/>).

229

230 ERA5 uses the IFS cycle 41r2 and it relies on land surface model and assimilation
231 configuration that are consistent with those used for operational NWP with coupled land-
232 atmosphere simulations and the latest soil moisture and snow assimilation (see sections 2.1
233 and 2.2 above). ERA5 has a high resolution component at ~31 km which is used in this study
234 (hereafter called ERA5-HRES). In ERA5-HRES, variables (analysis and short range forecasts
235 generated at 06 and 18 UTC) are available hourly. Variables that are valid for a period, e.g.
236 precipitation or runoff with an accumulation time, are provided as hourly forecasts.

237

238 At the time of writing approximately 28 years of ERA5-HRES data was available in the
239 ECMWF MARS data archive in three separate periods: 1985-1987, 1989-1995 and 1999-
240 2016. The first years (1985, 1989 and 1999) were used as spin up years, so in total 25 years
241 of daily river discharge and other surface data could be processed for the analysis (hereafter
242 called ERA5-D25).

243

244 **2.7 Experimental set-up**

245 In the ONLINE experiment, the operational ERA5-HRES reanalysis data was used directly
246 from all three ERA5-HRES periods for land surface variables, including runoff, produced by
247 coupled land-atmosphere model with LDAS and an open water budget (figure 1). In the
248 OFFLINE experiment, on the other hand, three standalone HTESSEL runs were set up, one
249 for each of the periods, to reproduce the land surface variables in land surface only mode
250 without the impact of coupling and LDAS, but with a closed water budget. As ERA5 has a
251 recent model cycle (41r2), the same HTESSEL version could be used in the offline
252 experiment as in the operational ERA5.

253

254 In the ECMWF NWP system, there is no option currently to run the land-atmosphere
255 coupling and LDAS separately. Either both are active as in ONLINE, or neither of them as in
256 OFFLINE. It would be interesting to separate the impact of these two contributing modelling
257 options, but as they are too strongly interwoven the separation would require a very large
258 effort, which is outside of the scope of this study.

259

260 In the OFFLINE experiment, the offline HTESSSEL model was forced with hourly ERA5-
261 HRES atmospheric data, wherever it was possible on the lowest model level, with an hourly
262 model time step. The model was run on the original horizontal resolution of ERA5-HRES
263 (~31 km). For precipitation, temperature, specific humidity, wind speed and surface pressure
264 the hourly analysis fields were applied, while for radiation and precipitation fluxes the first
265 12-hour period of the 06:00 and 18:00 UTC short-range forecasts were used to cover each 24-
266 hour periods.

267

268 The river discharge was generated by routing the runoff using CaMa-Flood for both the
269 ONLINE and OFFLINE datasets over the ~25 km river network. CaMa-Flood was run with a
270 1-hour time step and a 24-hour output frequency to match the 24-hour reporting frequency of
271 the river discharge observations.

272

273 **2.8 River discharge observations**

274 In this study, daily river discharge observations used in the GloFAS system are selected.
275 These are mostly from the Global Runoff Data Centre (GRDC) archive, an international
276 depository of river discharge observations and associated metadata.

277

278 The observations consist of a network of approximately 900 river gauging stations with
279 upstream areas over 10,000 km², selected from the catchments used in Zsoter et al. (2016).
280 After visual inspection those catchments that showed a clear non-realistic behaviour and/or
281 influence of dams were excluded. A minimum of 9 years, with at least 330 days in each of
282 those calendar years, were selected as criteria for the stations to be included in the river
283 discharge analysis. This is quite a short period, but due to the limited availability in more
284 recent years, it was accepted as a compromise. In total 590 stations could be processed
285 globally leaving large blank areas mostly in Asia and Africa (Figure 3).

286

287 **2.9 Annual peak river discharge**

288 For the river discharge verification, the annual peak river discharges from the two ERA5-
289 HRES simulations were determined in each calendar year as the highest value in the ± 30 -day
290 window around the observed annual maximum river flow. The 30-day window was defined
291 as a safeguard to avoid detecting high skill with similar peaks in observation and simulation
292 of completely different flood waves at very different periods of the year.

293

294 **2.10 Water budget increments**

295 This study focuses on the impact of the water budget closure on river discharge. In order to
296 analyse this the daily (00-00 UTC) water budget error term (dA) was computed as:

$$dA = P - E - R - dS \quad (1)$$

297 where P is precipitation, E is evapotranspiration, R is runoff, all taken as the sum of the
298 hourly forecast values (24 in total) in the ONLINE experiment from the 00-00 UTC period
299 and dS is the change in the storage term (water content in the soil including all four layers
300 and also in the snow cover) computed as the difference between the two subsequent 00 UTC
301 analysis values in ONLINE (representing the change in the water content during the 24-hour

302 period). Even though the water budget error is zero in OFFLINE (the water budget is closed),
303 the contributing variables can help identifying the behaviour of the surface processes in both
304 the ONLINE and OFFLINE simulations.

305

306 The imbalance in the amount of water that is not accounted for in the ONLINE water budget
307 effectively comes from the snow depth and soil moisture increments in LDAS which remove
308 or add water in the system. The daily increments (valid for a 00-00 UTC 24-hour period) are
309 computed as the sum of two increment values at 06 and 18 UTC (each day). Both of these
310 increments are computed as the ERA5-HRES analysis value minus the corresponding 12-
311 hour ERA5-HRES forecast value (initialised 12 hours earlier).

312

313 **2.11 Daily 2-metre temperature and snow depth**

314 The in situ surface synoptic observations (SYNOP) were used to verify 2-metre temperature
315 and snow depth for both the OFFLINE and ONLINE experiments. The observing stations
316 were filtered according to the station altitude difference to the model orography and only
317 those were used which had less than 150 metres discrepancy, as orography has control on
318 both variables and large differences would make the comparison unreliable. This maximum
319 orography difference value was chosen in accordance with the general practice at ECMWF,
320 where 100 metres is used to filter stations in the 2-metre temperature verification. For our
321 study, a less stringent compromise value was preferred in order to increase the sample size
322 and still guarantee good match between model and real orography.

323

324 2-metre temperature was verified for around local noon (Table 1), while for snow depth the
325 first measurement of the calendar day was evaluated in case of sub-daily records. In total,
326 observations from about 4000 stations for 2-metre temperature and 1500 stations for snow

327 depth were available for verification. For each catchment, a representative daily observation
328 was also determined for both variables. For catchments with more than one SYNOP station
329 available, these were calculated as the arithmetic average of the stations within the
330 catchment. It has to be acknowledged that the observation network available was not dense
331 enough to represent the full spatial variability of these surface variables, specially snow
332 depth, which vary dramatically in space from one point to another (Molotch and Bales,
333 2005). However, for a global study on the hydrological impacts it is expected to be sufficient.
334

335 **2.12 Climatologies**

336 Daily climatologies were used for river discharge and other surface variables in this work for
337 both observations and the two simulations. These data sets were produced with all potentially
338 available 25 years of data in ERA5-D25, always matching the number of available nearly
339 complete calendar years (with minimum 330 river discharge observations) for all the
340 catchments. For each day of the year a 21-day window, centred over the day, was used which
341 provided a minimum of about 180 values in the climate sample (with the 9 years minimum
342 criteria). The only exception are 2-metre temperature and snow depth, where a fixed shorter
343 period of 2000-2007 was used without the criteria of nearly complete years. As the 2-metre
344 temperature and snow depth observation availability is much better in more recent periods
345 and also less prone to missing values than river discharge, a shorter fixed period (when
346 ERA5-HRES was available) is sufficient.

347

348 **2.13 Verification statistics**

349 A number of statistics were applied to evaluate the overall performance of the two
350 climatological simulations in ERA5-D25 (Table 2). Several scores were selected in order to
351 give a more representative description of the general behavior including the differences

352 between the ONLINE and OFFLINE experiments. This is recommended e.g. by Legates and
353 McCabe (1999) as different scores demonstrate different aspects of the model attributes
354 ultimately providing a more complete picture.

355

356 The climatological daily time series were compared to the observed data using mean error
357 (ME), mean absolute error (MAE), Nash-Sutcliffe model efficiency (NSE; Nash and Sutcliffe
358 1970) and also Pearson correlation coefficient (R; Pearson 1896) in order to measure the fit
359 between model and observations. In addition, the mean and standard deviation of the
360 observed and modelled values were analysed with four additional indices, the percentage
361 sample mean error, the percentage sample mean absolute error, the percentage sample
362 standard deviation error and the percentage sample standard deviation absolute error.

363

364 Another very important aspect of hydrological model verification is the ability of the systems
365 to correctly predict the extremes, as these events can cause the highest impact. To measure
366 this, the timing and magnitude errors of the annual peaks were considered. Both the ME and
367 MAE measures (mean of all years in the sample) were computed for the timing and for the
368 percentage magnitude errors using the annual peaks over the 25 analysed years (for details on
369 how the annual peaks were computed see Section 2.9). For the analysis of the data
370 assimilation impact on 2-metre temperature and snow depth the ME and MAE scores were
371 used. In this study verification was conducted on homogeneous samples across all compared
372 scores for all the verified surface variables.

373

374 **3 Results**

375 The river discharge behaviour provides a useful indication of the hydrological differences
376 between the ONLINE and OFFLINE simulations. However, in order to understand the

377 underlying processes better, the coupling and LDAS impact was also analysed globally and
378 regionally based on the water budget and the related surface variables.

379

380 **3.1 Snow depth and 2-metre temperature impact**

381 The LDAS is designed to provide adequate initial surface conditions to the NWP forecasts.

382 The impact on the hydrology could be demonstrated on two important surface variables: 2-
383 metre temperature and snow depth (at least in snow impacted areas) which are relatively well
384 observed variables and can be used to analyse the impact of the land-atmosphere coupling
385 and LDAS on the surface globally in the two experiments. For details on how the
386 observations were used please see Section 2.11.

387

388 The picture for 2-metre temperature is rather mixed geographically with an overall MAE
389 improvement in ONLINE of around 0.3-0.4 °C as a global average up to 1-2 °C locally (not
390 shown). This corresponds to about 20-30% decrease in MAE on average in ONLINE, with
391 the impact of coupling and LDAS, compared to OFFLINE.

392

393 The improvement in the snow depth, which has much larger direct impact on the hydrology,
394 is more pronounced, based on the stations used in this study. The errors in ONLINE are
395 significantly reduced with most stations showing below $\pm 1-2$ cm ME (not shown), and
396 decrease of MAE by as much as 10-20 cm in some of the snow dominant locations in the 50-
397 70 latitude band (Figure 4). This is a very large improvement in ONLINE by removing 70-
398 80% (as global average) of the errors found in the OFFLINE experiment. Countries of
399 Central America, including Mexico, Venezuela and Columbia, tend to provide snow
400 information in their SYNOP observations. In these regions both the model and the in situ
401 stations mostly indicate snow free conditions, leading to very low MAE as shown in Figure 4.

402 Although the improvements are large, this does not necessarily mean that the simulation is
403 generally better. In situ snow observations are associated to potential representativeness
404 issues, particularly in mountainous areas. When assimilating a non-representative dataset at a
405 coarse special scale, the results can potentially degrade, even though the match to the actual
406 observations is better (Molotch and Bales, 2015). As the 2-metre temperature and snow depth
407 observations used in this study for verification were also assimilated in ERA5, the result will
408 favour to some extent the ONLINE experiment.

409

410 **3.2 Global water budget analysis**

411 The water budget is closed in OFFLINE by design, while in ONLINE the LDAS increments
412 can add or remove water, which could potentially lead to large errors in the budget over a
413 long period. The first aspect that was important to check is the amount of water that is lost or
414 gained in a day on average in the hydrological cycle.

415

416 Figure 5 shows the average daily water budget errors (Figure 5a) and the related snow water
417 equivalent (Figure 5b) and soil water content (Figure 5c) increments (for the definition of
418 these terms please see Section 2.10). In Figure 5, negative values (red) indicate water
419 removal by LDAS, while positive values (blue) show where water is added to the
420 hydrological cycle.

421

422 The three figures highlight significant biases in the ONLINE experiment as these water
423 budget errors represent generally $\pm 10\text{-}25\%$ of the total precipitation with locally even higher
424 ratios (not shown). In addition, at latitudes higher than 50 degrees North the dominant pattern
425 is a negative water budget error (Figure 5a). The major contributing factor to the clearly
426 negative errors in this area is the correction of snow pack with LDAS removing snow to

427 account for possible inaccuracies in the HTESSSEL snow scheme (Figure 5b). On average
428 snow water increments are negative almost everywhere where snow is present. The only
429 notable exception is in Canada where some central areas have positive water budget errors
430 which could possibly come from a negative precipitation bias that needs to be compensated
431 by LDAS.

432

433 Other areas of the world, the central USA, most of Amazonia, Africa, south Asia with India
434 and also large parts of Australia show positive errors in Figure 5a, where extra water is added
435 by LDAS. However, the positive errors are not exclusive as large parts of China, southeast
436 US and areas in central South-America experience negative water budget errors in these
437 mostly warm climatic conditions. Most of these increments come from the soil moisture
438 assimilation impact (Figure 5c). The soil moisture assimilation can generally compensate for
439 precipitation or 2-metre temperature biases. For example, if the 2-metre temperature is too
440 low, the assimilation will remove water, therefore reducing evaporative cooling which
441 subsequently increase the temperature in general.

442

443 **3.3 Catchment-level process examination**

444 To demonstrate how HTESSSEL handles the land surface processes with and without coupling
445 and LDAS, an in-depth case study analysis of the annual water budget cycle was performed
446 for an example catchment on the Amur river in east Russia (see Figure 6, catchment no.13).
447 This catchment is heavily snow impacted during winter and can demonstrate nicely the
448 important aspects of the hydrological cycle behaviour with the LDAS in action.

449

450 In the HTESSSEL hydrological cycle representation the input precipitation combined with the
451 melted part of the snowpack (snowmelt) is distributed into evapotranspiration, runoff (as sum

452 of surface and sub-surface runoffs), snow water storage (falling snow part of the
453 precipitation) and soil water storage (soil moisture in the four soil layers). The daily water
454 budget error, computed as in Eq. 1 (without the snowmelt separated), is zero in OFFLINE,
455 while ONLINE can show errors due to the increments adding or removing water. Figure 7
456 summarises the annual cycle of all the water budget contributing variables.

457

458 The displayed variables are daily climatological means calculated as described in Section
459 2.12. The following variables are shown in Figure 7: simulated precipitation (same for both
460 experiments), evapotranspiration, runoff, soil water and snow water storage terms (in Eq. 1)
461 for both ONLINE and OFFLINE; snow and soil water content increments for ONLINE;
462 simulated snowmelt, snow depth and river discharge for both the ONLINE and OFFLINE
463 experiments, and finally the corresponding river discharge and snow depth observations.

464

465 Figure 7 shows that for the Amur the ONLINE simulation significantly improves the
466 representation of snow depth, but as consequence, by the snow assimilation removing a lot of
467 snow, it drastically reduces the river discharge peak seen during the snowmelt season. The
468 explanation of this conclusion with detailed analysis of the evolution of the different surface
469 variables in the different seasons is given in the following:

470

- 471 • **Winter:** During December to February there is relatively little activity. The little
472 amount of precipitation falls mostly as snow, building the snowpack. Some snow is
473 removed by the assimilation through the small negative snow increments. Water
474 leaves the bottom of the soil as sub-surface runoff with hardly any surface runoff. The
475 OFFLINE simulation is generally similar to ONLINE, but snow depth bias shows
476 increasingly positive values in OFFLINE due to the extra amount of water going into

477 the snowpack in the OFFLINE experiment from snowfall (especially during first half
478 of the winter).

479

480 • **Spring:** From March, there is a pronounced snowmelt period in the model, peaking at
481 the end of April, lasting until middle of June (with virtually zero snowpack in
482 catchment average after middle of May). The increased precipitation in this spring
483 period with the large amount of snowmelt increases the soil water content and also
484 results in larger surface runoff output in both experiments. However, the snowmelt is
485 much smaller in ONLINE during April-May as a direct consequence of the large
486 negative snow increments (peaking early April) removing snow in the ONLINE
487 experiment. Similarly, due to the smaller amount of available water in ONLINE, the
488 surface runoff is also significantly smaller mainly in April/May. The snow depth
489 errors peak in middle of March by about 5 cm in OFFLINE with no errors in
490 ONLINE (as catchment average). The data assimilation rightly corrects this
491 substantial positive snow bias, however, the removed snow will be missing from the
492 water cycle as is highlighted by the unnoticeable spring peak river flow, which is
493 higher in the OFFLINE simulation mainly due to the extra snowmelt.

494

495 • **Snowmelt problem:** This behaviour of HTESSSEL with LDAS is rather surprising and
496 at first it might sound as a contradiction. How can the correct snow conditions lead to
497 such poor river discharge in the ONLINE experiment? A possible explanation could
498 be the representativeness issue of some of the snow observations, which can
499 potentially cause local degradation in some of the catchments. It can also be explained
500 by the HTESSSEL tendency to melt the snow too slowly (Dutra et al. 2012). In its
501 simple, single layer snow scheme, too much snow accumulates into the snow pack

502 and then that snow melts too slowly. For example, during a 20 mm mixed snow/rain
503 forecast event (10 mm liquid and 10 mm solid) the snow scheme will accumulate
504 most of the 10 mm solid (snow) part of the precipitation into the snowpack regardless
505 of the temperature conditions and melt only a little of this 10 mm. However, in reality
506 a lot of that rain, sleet or wet snow would not accumulate on the ground, and instead
507 most of it would melt straightaway. It seems the OFFLINE simulation gets the river
508 discharge right mainly for the wrong reasons. Although the snowpack is clearly more
509 poorly represented, the better timing with the delayed snowmelt (through the too slow
510 melting) and the extra water in the snowpack, the OFFLINE experiment gets the
511 runoff peak more correct.

512

513 • **Summer:** The water budget is balanced between precipitation and evapotranspiration
514 with some soil water increments. During early summer water is taken out of the soil to
515 cover the higher evapotranspiration. In OFFLINE more water leaves the soil which
516 increases the runoff and also evapotranspiration. By August, however, the excess
517 water from precipitation over evapotranspiration goes again into the soil which is
518 more pronounced in ONLINE where the soil is drier. The end of summer river
519 discharge peak is present in both simulations with the OFFLINE showing a better
520 peak due to more water in the soil and subsequently higher surface and sub-surface
521 runoff during all summer. The OFFLINE river discharge exceeds the ONLINE values
522 all summer and the two will level out by September, when the runoffs become similar
523 in the two experiments.

524

525 • **Autumn:** From the middle of September there is another smaller snowmelt period
526 starting with the falling temperatures and bringing some negative snow increments in

527 the ONLINE simulation. The snow accumulates into the snowpack in both
528 experiments, but again with a higher rate in OFFLINE, and also with larger snowmelt
529 amounts in OFFLINE.

530

531 **3.4 Regionally representative catchments**

532 In the previous section the LDAS response was highlighted for an important weakness of
533 HTESSEL with significant consequences on river discharge. In the following, the land-
534 atmosphere coupling and LDAS impact is now demonstrated with a simplified representation
535 of the annual water cycle in different geographical areas and also various climatic conditions
536 for a selection of the world's catchments in Figure 8. The displayed variables are simulated
537 snowmelt, evapotranspiration and river discharge in both the ONLINE and OFFLINE
538 experiments, the snow and soil water increments for ONLINE and finally the river discharge
539 observations. All values are daily climatological mean values as in Figure 7. The location of
540 the catchments is provided in Figure 6.

541

542 In Figure 8, twelve catchments are selected to represent all main areas of the world where
543 river discharge observations are available. Many of them are very large rivers, some of the
544 catchments are dominated with mixed snow and soil moisture influence from the Northern
545 Hemisphere while others, mainly in the tropics, are only soil moisture impacted. In table 3,
546 the main catchment details are provided, complemented with the NSE and the percentage
547 peak magnitude ME and MAE values for the catchments. The scores favouring the ONLINE
548 experiment are displayed with bold numbers.

549

550 Figure 8 suggests that the decreased snowmelt is a general feature in ONLINE across the
551 Northern Hemisphere as predicted already by Figure 5b. All displayed catchments have

552 generally lower river discharge in ONLINE, either concentrated over the high river discharge
553 season (e.g. Ob (no. 1) and Yukon (no. 2)), or elongated over most of the year (e.g. Danube
554 (no. 3) and Rhine (no. 4)). The snowmelt is universally smaller in the ONLINE simulation,
555 with the LDAS removing snow at different periods of the year, which seems to be the driving
556 force behind the river discharge differences.

557

558 The decreased amount of water has a mixed river discharge skill impact. For some
559 catchments (Ob (no. 1), Yukon (no. 2), Columbia (no. 6), and the case study catchment on the
560 Amur (no. 13)) the change during the high river discharge season is disadvantageous in
561 ONLINE, confirmed by mostly negatively impacted scores, such as the NSE and the
562 percentage peak magnitude MAE values in Table 3. On the other hand, for the Mississippi
563 (no. 5), Danube (no. 3) and Rhine (no. 4) it is rather beneficial as the daily climatological
564 mean river discharge is closer to the corresponding observations during the high season,
565 accompanied with mainly positive skill changes in the ONLINE experiment as both NSE and
566 percentage peak magnitude MAE improves (Table 3), except the Rhine catchment (no. 4)
567 where the percentage peak magnitude MAE deteriorates.

568

569 In the warm climate, however, where soil water dominates the land surface processes (Xingu,
570 Amazon, Hadejia, Ubangi, Zambesi and Flinders (no. 7-12)), the land-atmosphere coupling
571 and LDAS impact on river discharge seems to be smaller than for the snow influenced
572 catchments, and on evapotranspiration it tends to be larger. There are large biases over five of
573 the six highlighted tropical catchments (the only exception of the Flinders river in Australia),
574 where both the ONLINE and OFFLINE experiments show significant mismatch with the
575 observed values for the total river discharge volume and also for the annual peaks. For
576 example, as displayed in Table 3, on the Hadejia river in Nigeria the percentage peak

577 magnitude ME is 297% (the simulation is almost three time higher than the observation) in
578 ONLINE which is significantly better than OFFLINE (the improvement is 139% in the
579 percentage peak magnitude MAE). This points to the fact that even though the river discharge
580 differences are smaller in relative terms, it can still lead to noticeable change in the scores for
581 some of these highlighted catchments (Table 3).

582

583 Even though there is no clear systematic difference between the exclusively soil moisture and
584 the mixed (snow and soil moisture) catchments in terms of river discharge skill impact, the
585 snow clearly looks to carry a more direct influence on the river discharge volume and also on
586 the river discharge skill.

587

588 **3.5 Global river discharge analysis**

589 In the previous sections it could be shown that the water budget is out of balance in the
590 ONLINE simulation over large parts of the world leading to significant impact on the river
591 discharge for the analysed list of catchments. As an extreme example, it was demonstrated
592 that the snowmelt driven spring river discharge peak was almost completely missed in a large
593 catchment in east Russia in ONLINE. After the individual catchment examples, a systematic
594 analysis of the river discharge quality in the ONLINE and OFFLINE experiments is provided
595 based on all available catchments globally.

596

597 Although a large number of scores were computed in this study, this section will focus only
598 on the annual peak flow scores. The timing and magnitude of the high river discharges are
599 both crucial aspects of river discharge simulations in any flood prediction system such as
600 GloFAS. The accurate simulation of the river discharge peaks is essential to get the best
601 possible guidance for the potentially most damaging floods. The analysed performance of the

602 annual peak river flows should give a good indication on the general ability of the two
603 experiments to predict peaks.

604

605 Figure 9a highlights a large systematic percentage peak magnitude ME in the ONLINE
606 simulation. Many catchments show over 50% error (either positive or negative) of the annual
607 river discharge peaks on average. The majority of the Northern Hemispheric higher latitudes
608 is overwhelmingly under predicted, while Amazonia, western USA and also many
609 catchments in Africa are over predicted in the ONLINE experiment. The geographical pattern
610 in Figure 9a is rather similar to the one seen in Figure 5a. Most of the catchments with
611 significant negative values over the Northern Hemisphere and positive ones mainly in lower
612 latitudes, do resemble well the water budget error pattern seen in Figure 5a.

613

614 The water budget imbalance, caused by the increments in LDAS, is only one of the many
615 potential contributing factors to peak river flow errors (and in fact to general river discharge
616 errors); atmospheric forcing biases, imperfect river routing and observation errors could also
617 lead to large inaccuracies (Zhao et al. 2017).

618

619 The impact of the land-atmosphere coupling and LDAS seems to decrease the amount of
620 water overwhelmingly in the rivers (decreased sample mean river discharge, not shown). The
621 sample average river discharge increased only in the southern half of Brazil, in the central
622 part of Canada and one or two catchments in Africa, East Asia and South Australia (not
623 shown). It is expected that the decreased average river discharge in ONLINE should
624 generally also result in lower annual peak river flows over most of the globe. Figure 9b
625 shows that this decreasing tendency of the annual peaks in the ONLINE experiment coincides
626 with widespread, quite large deterioration in the percentage peak magnitude MAE score

627 (increase of the annual peak magnitude errors) especially in Asia and Europe and the north
628 western part of North America, where the majority of the catchments show significant
629 negative bias in Figure 9a. On the other hand, quite a few catchments seem to benefit from
630 the coupling and LDAS as the annual peak errors decrease especially in the western parts in
631 North America, where there is a large cluster of catchments with noticeably smaller
632 percentage peak magnitude MAE.

633

634 The river discharge peak timing bias in the ONLINE simulation is dominantly positive (peaks
635 are too late) in the Northern Hemisphere and mainly negative (peaks too early) in the Tropics
636 (not shown). However, the coupling and LDAS do not seem to have any systematic impact
637 on this aspect of the peak river flows. There are noticeable differences but they have no
638 distinguishable geographical pattern (not shown). It seems the short time series (9-25 annual
639 values only) were not sufficient to extract any representative timing differences between the
640 two experiments.

641

642 In addition to the analysis of the annual river discharge peak performance, the general fit
643 between modelled and observed daily river discharge time series is also extensively measured
644 by several scores. Table 4 shows a global summary giving an indication on the overall
645 performance of the two experiments. The scores are calculated as global averages weighted
646 by the square root of the catchment area size. This way a more representative picture can be
647 provided by giving more emphasis on the larger catchments.

648

649 The generally decreasing amount of water leads to larger differences for most of the volume
650 related bias scores. The percentage sample ME, the percentage sample standard deviation
651 error and also the percentage peak magnitude ME scores all decrease significantly in the

652 ONLINE simulation, bringing the global biases closer to zero. The only exception is the
653 discharge ME score which changes from a positive value to a negative one with similar
654 magnitude. The better biases, however, do not necessarily help improving the river discharge
655 skill globally; the scores presented in Table 4 provide a mixed picture, with some favouring
656 the ONLINE while others the OFFLINE simulation. This agrees with the mixed scores shown
657 in Table 3 for the regional example catchments. In general, the MAE, R, the percentage
658 sample MAE and the percentage peak magnitude MAE values are all slightly better for
659 OFFLINE, while the NSE and percentage sample standard deviation absolute error show
660 improvement for ONLINE. And finally, the peak timing ME is slightly better for the
661 OFFLINE experiment, while there is no difference in the global average peak timing MAE.

662

663 **4 Discussion**

664 In Section 3, the land-atmosphere coupling and LDAS impact on hydrology, including river
665 discharge and the related water budget variables was analysed. The river discharge scores
666 showed a mixed picture between the ONLINE and OFFLINE simulations with relatively
667 similar global performance. Larger differences could be highlighted in certain regions, such
668 as many of the snow dominant catchments in the Northern Hemisphere, where over many
669 areas a large amount of water is missing from the hydrological cycle and causing downstream
670 issues in river discharge especially during the snowmelt season in ONLINE.

671

672 The general decrease in the volume of water in the ONLINE experiment, mainly coming
673 from the snow dominated areas where the assimilation removes snow, seems to be the
674 primary impact on the hydrology. In soil moisture dominated areas the river discharge seems
675 to be less impacted by the increments and the evapotranspiration rate holds a more important
676 role.

677

678 Data assimilation is a very important component of any NWP system with a lot of effort and
679 research concentrated on the use of observations to correct for random (day-to-day) errors.

680 Data assimilation systems are not there to correct for systematic biases. The fact that LDAS
681 produces consistent negative increments in snow covered areas in this study is pointing
682 towards an apparent snow model bias. In contrast, a model affected by random errors only,
683 would lead to data assimilation increments of both signs with close to zero annual mean
684 values.

685

686 Other studies have also highlighted significant snow assimilation impacts on the water
687 balance. For example, De Lennoy et al. (2012) showed that on a small catchment in Colorado
688 (USA) the season averaged snowpack water content is largely decreased by the snow water
689 equivalent assimilation in the Noah land surface model, and could only be overcome by
690 scaling applied (to anomalies) to the observations prior to assimilation. Similarly, Arsenault
691 et al. (2013) found that assimilating MODIS snow cover fraction observations into the CLM
692 land surface model by a simple rule-based direct insertion and the one-dimensional ensemble
693 Kalman filter methods, lead to substantial snowpack removal (without melting, thus causing
694 negative bias in runoff), by both methods in Colorado and Washington.

695

696 In the ECMWF system, the snow increments are correcting for the systematic overestimation
697 of the current HTESSEL snow scheme which melts the snow too slowly. Dutra et al. (2012)
698 highlighted that although the current snow scheme provides a significant improvement over
699 the previous one, it does not yet improve on the short-duration melting events during late
700 winter and spring. They argued that the experimental multi-layer snow scheme was able to

701 reproduce, at least partially, those snowmelt episodes thanks to the top snow layer having a
702 reduced thermal inertia.

703

704 The findings in this work are specific to the NWP configuration at ECMWF with the
705 HTESSEL land surface model and the processes within. However, any LSM's ability to
706 support hydrological simulations can be limited by inadequate handling of the processes,
707 potentially causing a similar problem downstream in the hydrology. The areas highlighted
708 here for ECMWF's HTESSEL in supporting the flood forecasting activities can be improved
709 by some potential developments in the future. Some of the areas where substantial
710 improvements could be achieved are described in the following below:

711

712 • A new multi-layer snow scheme is currently being tested at ECMWF which is similar
713 to the one evaluated in Dutra et al. (2012). This improved snow scheme is expected to
714 represent better the snow melt processes and therefore reduce the snow increments
715 that currently remove a significant amount of water from the hydrological cycle. The
716 hydrological context developed in this study will be used to aid this development of
717 the new scheme.

718

719 • Another potential way of improving HTESSEL performance for hydrological
720 applications would be to modify the LDAS by special handling of the snow
721 increments in order to retain the water in the hydrological cycle during the data
722 assimilation. For example, Zaitchik and Rodell (2009) proposed an interesting
723 approach using near-future, snow-covered area observations to adjust the air
724 temperature and precipitation forcing data in order to preserve the local hydrological
725 balance. In another study, Pan and Wood (2006) developed a constrained ensemble

726 Kalman filter method to assure closure of the water balance when assimilating
727 hydrological observations. These types of studies rely on uncoupled systems and they
728 would be difficult to implement in operational, real-time environment. However, they
729 provide some insight on water budget closure in data assimilation, and they should be
730 further investigated and adapted to coupled land-atmosphere NWP systems. On the
731 longer term, further coupling between NWP and hydrological forecasting systems will
732 be considered, opening thereby the possibility for coupled land-hydrology data
733 assimilation. In this context, joint assimilation of land surface and river discharge
734 observations will consistently correct the different components of the Earth System.

735

736 • In addition, the land surface development methodology including data assimilation
737 techniques and process representation is continuously improved at ECMWF. The
738 future inclusion of the LDAS scheme in the offline HTESSSEL is in development. It
739 will create an environment where the offline research work, including the reanalysis
740 improvements (e.g. ERA5), could be done in a consistent way with the real-time
741 forecast generation. In parallel to these developments, addressing the water budget
742 closure in land-atmosphere data assimilation systems should be a priority in the future
743 to ensure consistent high quality coupled NWP and hydrological forecasts.

744

745 GloFAS is one of the few existing flood forecasting systems that utilises an LSM
746 (HTESSSEL) for representing the hydrology (Emerton et al. 2016). Although we acknowledge
747 that in some cases a simple routing model, initialised from observed upstream river levels
748 (either from river gauges or satellite measurements), could be a simpler alternative to
749 simulate downstream discharge on large rivers a few days in advance, e.g. in Hossain et al.
750 (2014); in other cases where forecasts are required further in advance or where observations

751 are unavailable or of too low quality, a more complex modelling configuration, which
752 represents hydrological fluxes, becomes essential. Regardless of some limitations (e.g. the
753 one highlighted in the ECMWF NWP configuration), these complex models play crucial
754 roles in harnessing the available predictability in the land-atmosphere system.

755

756 **5 Conclusions**

757 Understanding the impacts of both the data assimilation and land surface process
758 representation in land surface models on simulated hydrological variables is very important,
759 not only for improving the weather and climate forecasts, but specifically for supporting
760 flood forecasting and other hydrological applications such as drought forecasting, and also
761 for giving feedback about the Earth System. In this paper, the influence of land-atmosphere
762 coupling and land data assimilation on global hydrological simulations from LSMs was
763 evaluated. Two river discharge simulations from two climatological reanalyses (based on
764 ERA5) were compared: one operational set which includes land-atmosphere coupling and
765 LDAS with an open water budget, and also an offline HTESSEL set with a closed water
766 budget and no LDAS.

767

768 It was found that while the ONLINE version of the model largely improves the 2-metre
769 temperature and snow depth conditions, it is causing poor representation of peak river flow in
770 snowmelt-dominated areas, particularly in the high latitudes. However, there are localised
771 improvements to peak river flow, such as in the western United States. The LDAS increments
772 remove or add water even on an annual average scale which inevitably leads to systematic
773 water budget errors and subsequently contribute to significant errors in river discharge during
774 times of peak flow downstream, something that is critical during times of flooding.

775

776 **Implications for hydrological forecasting:** This study has highlighted the impact of using
777 land data assimilation in reanalysis products. Where data assimilation is adjusting snowpack
778 in forecasting mode then there will also be important implications for hydrological
779 predictions. Future studies should address how far ahead the impact of data assimilation
780 propagates in hydrological forecasts. In addition, hydrological forecasting systems often use
781 initial river conditions derived from climatology. In these circumstances using climatological
782 products derived using data assimilation methodologies could lead to issues with the
783 hydrological forecasts. There are also related issues for forecasting systems such as GloFAS
784 which compare model output to climatology to provide early awareness of extreme events –
785 consistency between operational and climatological configurations goes some way to bypass
786 this problem, and this conclusion has directly influenced the design of the new GloFAS-
787 seasonal system (Emerton et al. 2018).

788

789 **Implications for land surface modelling and data assimilation:** Data assimilation is
790 designed to compensate for noise errors and not systematic bias. In the case of the current
791 HTESSEL snow assimilation scheme it is doing the latter; compensating for system
792 deficiencies such as the slow snowmelt process. This paper has discussed potential ways of
793 addressing water budget deficiencies in land surface approaches, for example including
794 multiple layers within the HTESSEL snow scheme or moving towards data assimilation that
795 conserves the water budget.

796

797 Without addressing such issues there will never be confidence in using LSMs for
798 hydrological forecasting applications across the globe. This type of analysis should be used to
799 diagnose where improvements need to be made; considering the whole Earth System in data

800 assimilation and coupling developments is critical for moving towards the goal of holistic
801 Earth System approaches.

802

803 **6 Acknowledgements**

804 Ervin Zsoter's PhD is supported by the Wilkie Calvert Co-Supported PhD Studentships at the
805 University of Reading. Ervin Zsoter was supported by the Copernicus Emergency
806 Management Service - Early Warning Systems (CEMS-EWS (EFAS)). Hannah Cloke is
807 supported by the TENDERLY project: Towards END-to End flood forecasting and a tool for
808 Real-time catchment susceptibility UK NERC Flooding From Intense Rainfall (FFIR)
809 programme, NE/K00896X/1. Elisabeth Stephens and Hannah Cloke are supported by the
810 FATHUM project: Forecasts for Anticipatory Humanitarian Action funded by UK NERC
811 as part of their Science for Humanitarian Emergencies & Resilience (SHEAR) programme,
812 NE/P000525/1. We are also grateful to The Global Runoff Data Centre, 56068 Koblenz,
813 Germany for providing the observation dataset for our river discharge analysis.

814

815 **7 Author contributions**

816 Ervin Zsoter designed the experiment, produced the ERA5-D25 data sets, carried out the
817 river discharge data analysis and led the writing of the manuscript. Hannah Cloke and Liz
818 Stephens assisted with posing the research question, and designing the analysis, Patricia and
819 Joaquin helped with the scientific analysis of data assimilation and coupling issues, Christel
820 Prudhomme and Florian Pappenberger helped design the research methodology. All authors
821 assisted with writing the manuscript.

822

823 **8 References**

824 Albergel C., P. de Rosnay, G. Balsamo, L. Isaksen and J. Muñoz Sabater, 2012: Soil moisture

825 analyses at ECMWF: evaluation using global ground-based in situ observations, J.
826 Hydrometeor., 13, 1442-1460, <https://doi.org/10.1175/JHM-D-11-0107.1>.
827
828 Alfieri, L., P. Burek, E. Dutra, B. Krzeminski, D. Muraro, J. Thielen, and F. Pappenberger,
829 2013: GloFAS - global ensemble streamflow forecasting and flood early warning, Hydrology
830 and Earth System Sciences, **17**, 1161–1175, <https://doi.org/10.5194/hess-17-1161-2013>.
831
832 Agustí-Panareda, A., G. Balsamo, and A. Beljaars, 2010: Impact of improved soil moisture
833 on the ECMWF precipitation forecast in West Africa, Geophys. Res. Lett., 37, L20808,
834 <https://doi.org/10.1029/2010GL044748>.
835
836 Andreadis, K., and D. Lettenmaier, 2006: Assimilating remotely sensed snow observations
837 into a macroscale hydrology model, Advances in Water Resources, 29(6), 872-886,
838 <https://doi.org/10.1016/j.advwatres.2005.08.004>.
839
840 Arsenault, K. R., P. R. Houser, G. J. M. De Lannoy, and P. A. Dirmeyer, 2013: Impacts of
841 snow cover fraction data assimilation on modeled energy and moisture budgets, J Geophys
842 Res - Atmos, <https://doi.org/10.1002/jgrd.50542>.
843
844 Balsamo, G., A. Beljaars, K. Scipal, P. Viterbo, B. van den Hurk, M. Hirschi, and A. K.
845 Betts, 2009: A Revised Hydrology for the ECMWF Model: Verification from Field Site to
846 Terrestrial Water Storage and Impact in the Integrated Forecast System, J. Hydrometeor., **10**,
847 623–643. <http://dx.doi.org/10.1175/2008JHM1068.1>.
848
849 Balsamo, G., S. Boussetta, P. Lopez, and L. Ferranti, 2010: Evaluation of ERA-Interim and

850 ERA-Interim-GPCP-rescaled precipitation over the U.S.A., Era report Series 01/2010, 10 pp,
851 ECMWF, Reading, UK.

852

853 Balsamo, G., F. Pappenberger, E. Dutra, P. Viterbo, and B. van den Hurk, 2011: A revised
854 land hydrology in the ECMWF model: a step towards daily water flux prediction in a fully-
855 closed water cycle, *Hydrol. Proc.*, **25**, 1046–1054, <https://doi.org/10.1002/hyp.7808>.

856

857 Balsamo, G., and Coauthors, 2015: ERA-Interim/Land: a global land surface reanalysis data
858 set, *Hydrol. Earth Syst. Sci.*, **19**, 389–407, <https://doi.org/10.5194/hess-19-389-2015>.

859

860 Bélair S., L.-P. Crevier, J. Mailhot, B. Bilodeau, Y. Delage, 2003: Operational
861 Implementation of the ISBA Land Surface Scheme in the Canadian Regional Weather
862 Forecast Model. Part I: Warm Season Results, *J. Hydrometeor.*, **4**, 352-370,
863 [https://doi.org/10.1175/1525-7541\(2003\)4<352:OIOTIL>2.0.CO;2](https://doi.org/10.1175/1525-7541(2003)4<352:OIOTIL>2.0.CO;2).

864

865 Beljaars A. C. M., P. Viterbo, M. Miller, A. K. Betts, 1996: The anomalous rainfall over the
866 United States during July 1993: Sensitivity to land surface parameterization and soil
867 anomalies. *Mon. Weather Rev.* **124**, 362–383.

868

869 Blyth, E., D. B. Clark, R. Ellis, C. Huntingford, S. Los, M. Pryor, M. Best, and S. Sitch,
870 2011: A comprehensive set of benchmark tests for a land surface model of simultaneous
871 fluxes of water and carbon at both the global and seasonal scale, *Geosci. Model Dev.*, **4**, 255-
872 269, <https://doi.org/10.5194/gmd-4-255-2011>.

873

874 Brasnett B., 1999: A global analysis of snow depth for numerical weather prediction. *J Appl*

875 Meteorol 38:726–740, <https://doi.org/10.1175/1520->
876 0450(1999)038<0726:AGAOSD>2.0.CO;2.

877

878 Dee, D. P., and Coauthors, 2011: The ERA-Interim reanalysis: configuration and
879 performance of the data assimilation system, *Q. J. R. Meteorol. Soc.*, **137**, 553–597,
880 <https://doi.org/10.1002/qj.828>.

881

882 Drusch M, D. Vasiljevic P. Viterbo, 2004: ECMWF s global snow analysis: assessment and
883 revision based on satellite observations. *J Appl Meteorol* 43:1282–1294,
884 [https://doi.org/10.1175/1520-0450\(2004\)043<1282:EGSAAA>2.0.CO;2](https://doi.org/10.1175/1520-0450(2004)043<1282:EGSAAA>2.0.CO;2).

885

886 Drusch M., and P. Viterbo, 2007: Assimilation of screen-level variables in ECMWF’s
887 Integrated Forecast System: A study on the impact on the forecast quality and analyzed soil
888 moisture. *Mon. Weather Rev.* 135: 300–314, <https://doi.org/10.1175/MWR3309.1>.

889

890 Dutra, E., G. Balsamo, P. Viterbo, P. Miranda, A. Beljaars, C. Schär, and K. Elder, 2010: An
891 improved snow scheme for the ECMWF land surface model: description and offline
892 validation, *J. Hydrometeor.*, **11**, 899–916, <https://doi.org/10.1175/JHM-D-11-072.1>.

893

894 Dutra, E., C. Schär, P. Viterbo, and P. M. A. Miranda, 2011: Land-atmosphere coupling
895 associated with snow cover, *Geophys. Res. Lett.*, **38**, L15707,
896 <https://doi.org/10.1029/2011GL048435>.

897

898 Dutra, E., P. Viterbo, P. M. A. Miranda, and G. Balsamo, 2012: Complexity of snow schemes
899 in a climate model and its impact on surface energy and hydrology. *J. Hydrometeorol.*, 13,
900 521–538, <https://doi.org/10.1175/JHM-D-11-072.1>.
901

902 Emerton, R. E., and Coauthors, 2016: Continental and global scale flood forecasting
903 systems., *WIREs Water*, 3, 391–418, <https://doi.org/10.1002/wat2.1137>.
904

905 Emerton R., H. Cloke, E. Stephens, E. Zsoter, S. Woolnough, F. Pappenberger, 2017:
906 ‘Complex picture for likelihood of ENSO-driven flood hazard’. *Nature Communications*.
907 <https://doi.org/10.1038/NCOMMS14796>.
908

909 Emerton R., E. Zsoter, L. Arnal, H. Cloke, D. Muraro, C. Prudhomme, E. Stephens, P.
910 Salamon, and F. Pappenberger, 2018: Developing a global operational seasonal hydro-
911 meteorological forecasting system: GloFAS-Seasonal v1.0, *Geosci. Model Dev.*, 11, 3327-
912 3346, <https://doi.org/10.5194/gmd-11-3327-2018>, 2018.
913

914 Haddeland, I., and Coauthors, 2011: Multimodel estimate of the global terrestrial water
915 balance: Setup and first results., *J. Hydrometeorol.*, 12, 869–884,
916 <https://doi.org/10.1175/2011JHM1324.1>.
917

918 Helfrich SR., D. McNamara, B. Ramsay, T. Baldwin, and T. Kasheta, 2007: Enhancements
919 to, and forthcoming developments in the interactive multisensor snow and ice mapping
920 system, (IMS). *Hydrol Process* 21:1576–1586. doi:10.1002/hyp.6720
921

922 Hersbach H., and D. Dee, 2016: ERA5 reanalysis is in production, ECMWF Newsletter No.
923 147, pp. 7.
924
925 Hossain, F., A. H. M. Siddique-E-Akbor, S. Biancamaria, H. Lee, and C. K. Shum, 2014:
926 Proof of Concept of an Altimeter-Based River Forecasting System for Transboundary Flow
927 Inside Bangladesh, IEEE J. Sel. Topics Appl. Earth Observ., vol. 7, no. 2, pp. 587-601,
928 <https://doi.org/10.1109/JSTARS.2013.2283402>
929
930 Huffman, G. J., R. F. Adler, D. T. Bolvin, and G. Gu, 2009: Improving the Global
931 Precipitation Record: GPCP Version 2.1., Geophys. Res. Lett., **36**,
932 <https://doi.org/10.1029/2009GL040000>.
933
934 Kauffeldt, A., S. Halldin, F. Pappenberger, F. Wetterhall, C.-Y. Xu, and H. L. Cloke, 2015:
935 Imbalanced land surface water budgets in a numerical weather prediction system, Geophys.
936 Res. Lett., 42, 4411–4417, <https://doi.org/10.1002/2015GL064230>.
937
938 De Lannoy, G. J. M., R. H. Reichle, K. R. Arsenault, P. R. Houser, S. Kumar, N. E. C.
939 Verhoest, and V. R. N. Pauwels, 2012: Multiscale assimilation of Advanced Microwave
940 Scanning Radiometer-EOS snow water equivalent and Moderate Resolution Imaging
941 Spectroradiometer snow cover fraction observations in northern Colorado, Water Resources
942 Research, 48(1), <https://doi.org/10.1029/2011WR010588>.
943
944 Helmert J., A. Sensoy, R. Alvarado Montero, C. de Michele, P. de Rosnay, M. Dumont, D. C.
945 Finger, M. Lange, G. Picard, V. Potopova, S. Pullen, D. V. Schuler, and A. Nadir Arslan,
946 2018: Review of Snow Data Assimilation Methods for Hydrological, Land Surface,

947 Meteorological and Climate Models: Results from a COST HarmoSnow Survey,
948 Geosciences, 8(12), 489, <https://doi.org/10.3390/geosciences8120489>.
949
950 Legates, D. R., and G. J. McCabe Jr., 1999: Evaluating the use of “goodness-of-fit” Measures
951 in hydrologic and hydroclimatic model validation, *Water Resour. Res.*, 35(1), 233–241,
952 <https://doi.org/10.1029/1998WR900018>.
953
954 Mahfouf J-F., P. Viterbo, H. Douville, A.C.M. Beljaars, and S. Saarinen, 2000: ‘A revised
955 land-surface analysis scheme in the Integrated Forecasting System’. ECMWF Newsletter No.
956 88.
957
958 Mengelkamp, H.-T., K. Warrach, C. Ruhe, and E. Raschke, 2001: Simulation of runoff and
959 streamflow on local and regional scales. *Meteor. Atmos. Phys.*, **76**: 107–117.
960
961 Molotch, N. P. and R. C. Bales, 2005: Scaling snow observations from the point to the grid
962 element: Implications for observation network design, *Water Resour. Res.*, 41, W11421,
963 <https://doi.org/10.1029/2005WR004229>.
964
965 Nash, J. E., and J. V. Sutcliffe, 1970: River flow forecasting through conceptual models part I
966 — A discussion of principles. *Journal of Hydrology*. **10** (3), 282–
967 290, [https://doi.org/10.1016/0022-1694\(70\)90255-6](https://doi.org/10.1016/0022-1694(70)90255-6).
968
969 Overgaard, J., D. Rosbjerg, and M. B. Butts, 2006: Land-surface modelling in hydrological
970 perspective—A review, *Biogeosciences*, 3(2), 229–241, <https://doi.org/10.5194/bg-3-229->
971 2006.

972

973 Pan, M., and E. Wood, 2006: Data assimilation for estimating the terrestrial water budget
974 using a constrained ensemble Kalman filter, *Journal of Hydrometeorology*, 7(3), 534-547,
975 doi:10.1175/JHM495.1.

976

977 Pearson, K., 1896: Mathematical contributions to the theory of evolution: III. Regression,
978 heredity and panmixia. *Philosophical Transactions of the Royal Society of London Series A*,
979 187, 253–318.

980

981 Rabier, F., H. Järvinen, E. Klinker, J.-F. Mahfouf, and A. Simmons, 2000: The ECMWF
982 operational implementation of four dimensional variational assimilation. Part I: Experimental
983 results with simplified physics, *Q. J. R. Meteorol. Soc.*, 126, 1143–1170,
984 <https://doi.org/10.1002/qj.49712656415>.

985

986 Rabier, F., 2005: Overview of global data assimilation developments in numerical weather
987 prediction centres. *Q. J. R. Meteorol. Soc.*, 131, 3215 – 3233,
988 <https://doi.org/10.1256/qj.05.129>.

989

990 de Rosnay P., M. Drusch, D. Vasiljevic, G. Balsamo, C. Albergel, and L. Isaksen, 2013: A
991 simplified Extended Kalman Filter for the global operational soil moisture analysis at
992 ECMWF, *Q. J. R. Meteorol. Soc.*, 139, 1199-1213, <https://doi.org/10.1002/qj.2023>.

993

994 de Rosnay P., G. Balsamo, C. Albergel J. Muñoz-Sabater, and L. Isaksen, 2014: Initialisation
995 of land surface variables for Numerical Weather Prediction, *Surveys in Geophysics*, 35(3), pp
996 607-621,

997

998 de Rosnay P., L. Isaksen, M. Dahoui, 2015: Snow data assimilation at ECMWF, ECMWF
999 Newsletter no 143, pp 26-31.

1000

1001 Slater, A. G., and M. P. Clark, 2006: Snow data assimilation via an ensemble Kalman filter,
1002 *Journal of Hydrometeorology*, 7(3), 478-493, <https://doi.org/10.1175/JHM505.1>.

1003

1004 Stephens, E., J. J. Day, F. Pappenberger, and H. Cloke, 2015: Precipitation and floodiness,
1005 *Geophys. Res. Lett.*, 42, 10,316–10,323, <https://doi.org/10.1002/2015GL066779>.

1006

1007 van der Knijff, J. M., J. Younis, and A. P. J. de Roo, 2010: LISFLOOD: A GIS-based
1008 distributed model for river basin scale water balance and flood simulation, *Int. J. Geogr. Inf.*
1009 *Sci.*, 24, 189–212, <https://doi.org/10.1080/13658810802549154>.

1010

1011 Le Vine, N., A. Butler, N. McIntyre, and C. Jackson, 2016: Diagnosing hydrological
1012 limitations of a land surface model: application of JULES to a deep-groundwater chalk basin,
1013 *Hydrol. Earth Syst. Sci.*, 20, 143-159, <https://doi.org/10.5194/hess-20-143-2016>.

1014

1015 Wang, L. L, D. H. Chen, H. J. Bao, 2016: The improved Noah land surface model based on
1016 storage capacity curve and Muskingum method and application in GRAPES model.
1017 *Atmospheric Science Letters*, 17, 190–198. <https://doi.org/10.1002/asl.642>.

1018

1019 Wu, H., R. F. Adler, Y. Tian, G. J. Huffman, H. Li, and J. Wang, 2014: Real-time global
1020 flood estimation using satellite-based precipitation and a coupled land surface and routing
1021 model, *Water Resour. Res.*, 50, 2693–2717, <https://doi.org/10.1002/2013WR014710>.

1022

1023 Yamazaki, D., S. Kanae, H. Kim, and T. Oki, 2011: A physically based description of
1024 floodplain inundation dynamics in a global river routing model. *Water Resour. Res.*, 47,
1025 W04501, <https://doi.org/10.1029/2010WR009726>.

1026

1027 Zaitchik, B.F. and M. Rodell, 2009: Forward-looking assimilation of MODIS-derived snow-
1028 covered area into a land surface model. *J. Hydrometeor.*, 10, 130–148,
1029 <https://doi.org/10.1175/2008JHM1042.1>.

1030

1031 Zhao, F., T. I. Veldkamp, K. Frieler, J. Schewe, S. Ostberg, S. Willner, B. Schauburger, S. N.
1032 Gosling, H. M. Schmied, F. T. Portmann, and G. Leng, 2017: The critical role of the routing
1033 scheme in simulating peak river discharge in global hydrological models, *Environ. Res. Lett.*,
1034 12, 075003, <https://doi.org/10.1088/1748-9326/aa7250>.

1035

1036 Zsoter, E., F. Pappenberger, P. Smith, R. E. Emerton, E. Dutra, E. Wetterhall, D. Richardson,
1037 K. Bogner and G. Balsamo, 2016: Building a multi-model flood prediction system with the
1038 TIGGE archive. *J. Hydrometeor.*, <http://dx.doi.org/10.1175/JHM-D-15-0130.1>.

Longitude band	30W - 60E	60-150E	150-180E	120-180W	30-120W
~ local noon	12	6	00	00	18

1039 Table 1. Criteria for selecting daytime 2-metre temperature

1040

1041

Score	Description	Used for
ME	Mean error	Daily river discharge, snow depth and 2-metre temperature
MAE	Mean absolute error	Daily river discharge, snow depth and 2-metre temperature
NSE	Nash-Sutcliffe efficiency	Daily river discharge time series
R	Pearson correlation coefficient	Daily river discharge time series
PMnE	Percentage sample mean error	Whole river discharge sample
PMnAe	Percentage sample mean absolute error	Whole river discharge sample
PStE	Percentage sample standard deviation error	Whole river discharge sample
PStAe	Percentage sample standard deviation absolute error	Whole river discharge sample
PkTiMe	Peak timing mean error	Annual river discharge peaks

PkTiMae	Peak timing mean absolute error	Annual river discharge peaks
PPkMgMe	Percentage peak magnitude mean error	Annual river discharge peaks
PPkMgMae	Percentage peak magnitude mean absolute error	Annual river discharge peaks

1042

1043 Table 2. List of verification scores used in the analysis with a short description and also the

1044 areas where they were applied.

1045

No.	Station	River	Area (*1000 km ²)	NSE		PPkMgMe (%)		PPkMgMae (%)	
				ONLINE	OFFLINE	ONLINE	OFFLINE	ONLINE	OFFLINE
1.	Salekhard	Ob	2541	0.40	0.52	-55.0	-40.7	55.0	40.7
2.	Pilot station	Yukon	865	0.31	0.64	-64.7	-50.7	64.7	50.7
3.	Boogojevo	Danube	257	0.47	-0.43	-3.5	29.1	19.8	32.4
4.	Lobith	Rhine	163	0.45	0.05	-39.1	-14.8	39.1	18.5
5.	Viicksburg	Mississippi	2963	-0.02	-2.69	1.6	31.4	17.7	43.5
6.	Quincy	Columbia	663	0.25	0.54	-24.0	-7.6	27.5	20.2
7.	Boa Sorte	Xingu	207	-1.53	-0.85	159.0	147.9	159.0	147.9
8.	Obidos-Linigrafo	Amazon	4664	-0.17	-0.21	26.6	26.9	26.6	26.9
9.	Hadejia	Hadejia	22	-9.01	-11.85	297.1	436.1	297.1	436.1
10.	Bangui	Ubangi	496	-5.72	-6.17	162.8	159.1	162.8	159.1
11.	Katima Mulilo	Zambesi	331	-7.97	-6.70	196.6	183.0	196.6	183.0

12.	Walkers bend	Flinders	106	0.66	0.62	-24.5	-11.4	46.9	45.9
13.	Komsomolsk	Amur	1846	0.43	0.68	-33.5	-18.7	33.5	18.7

1046

1047 Table 3. Details of the 13 catchments analysed in Figure 7 (no. 13) and Figure 8 (no. 1-12)
1048 with the NSE, PPkMgMe (percentage peak magnitude ME) and PPkMgMae (percentage peak
1049 magnitude MAE) score values for the ONLINE and OFFLINE experiments based on the
1050 ERA5-D25 dataset. Bold scores denote better performance. For further details on the scores
1051 see Section 2.13.

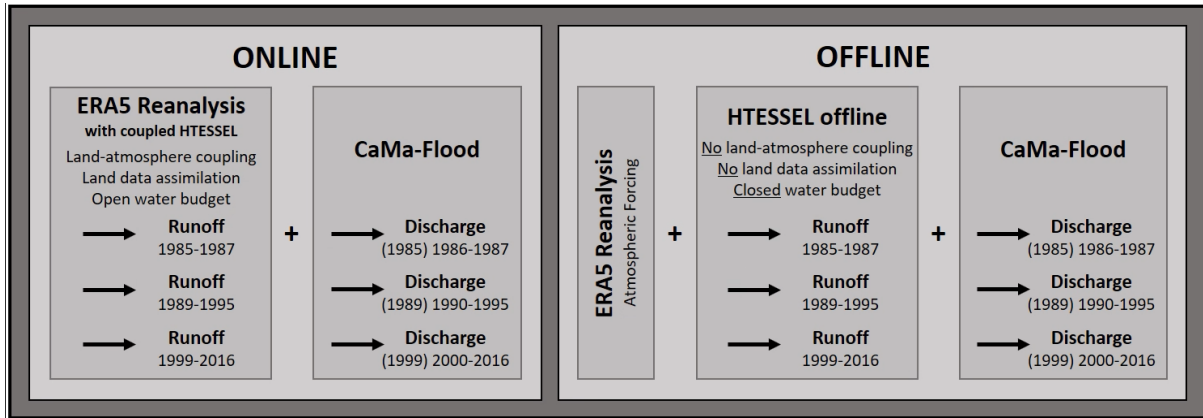
1052

Score	ME (m3/s)	MAE (m3/s)	NSE	R	PMnE (%)	PMnAe (%)	PStE (%)	PStAe (%)	PkTiMe (day)	PkTiMae (day)	PPkMgMe (%)	PPkMgMae (%)
ONLINE	-264	3017	-0.29	0.67	-2.6	29.0	9.6	48.3	-0.95	11.8	6.3	61.3
OFFLINE	236	2954	-0.53	0.70	16.9	27.2	34.2	52.1	-0.81	11.8	27.3	59.2

1053

1054 Table 4. List of global average scores for the ONLINE and OFFLINE experiments based on
1055 the ERA5-D25 dataset. Each value is a mean of scores from 590 catchments (where
1056 minimum of 9 years of river discharge observations was available) weighted by the square
1057 root of the catchment area sizes. For further details on the scores see Section 2.13. Bold
1058 numbers denote the better score of ONLINE and OFFLINE. The following scores are
1059 displayed: ME, MAE, NSE, R, Percentage sample mean error (PMnE), Percentage sample
1060 mean absolute error (PMnAe), Percentage sample standard deviation error (PStE), Percentage
1061 sample standard deviation absolute error (PStAe), Peak timing ME (PkTiMe), Peak timing
1062 MAE (PkTiMae), Percentage peak magnitude ME (PPkMgMe), Percentage peak magnitude
1063 MAE (PPkMgMae).

1064



1065

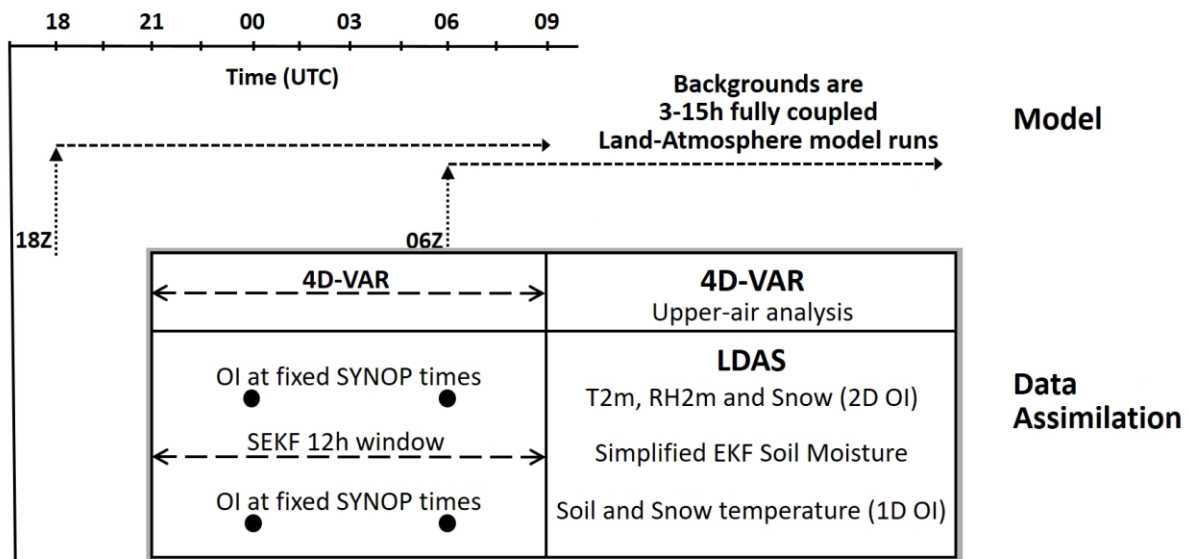
1066

Figure 1. Schematic of the ONLINE and OFFLINE experiments that were carried out to produce the ERA5-D25 dataset. The years in brackets for the discharge indicate the first spin-up year in each period that were excluded from the analysis.

1067

1068

1069

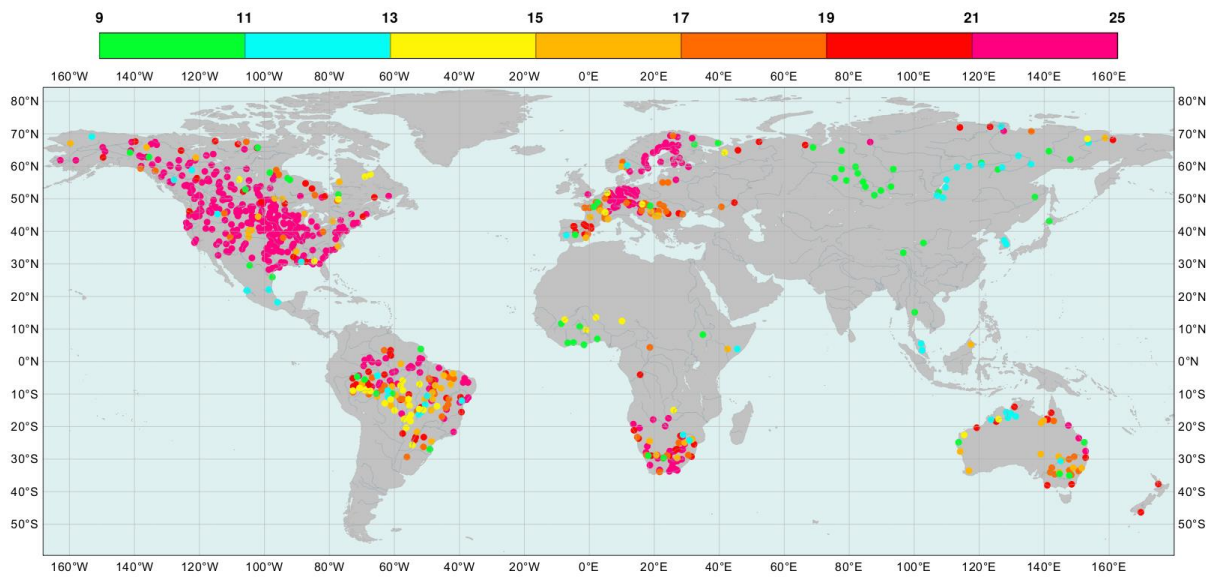


1070

1071

Figure 2. Schematic diagram of the land data assimilation system at ECMWF.

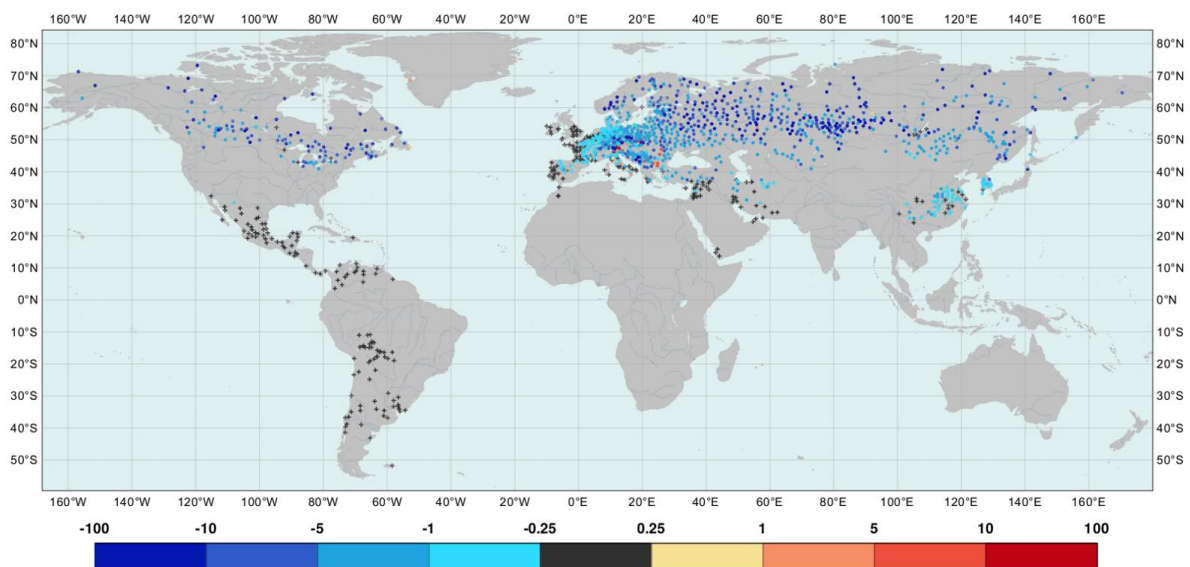
1072



1073

1074 Figure 3. Geographical distribution of river discharge observations with sufficient record
 1075 length selected for the analysis. Colours indicate the length of the available data in years
 1076 (from 9 to 25).

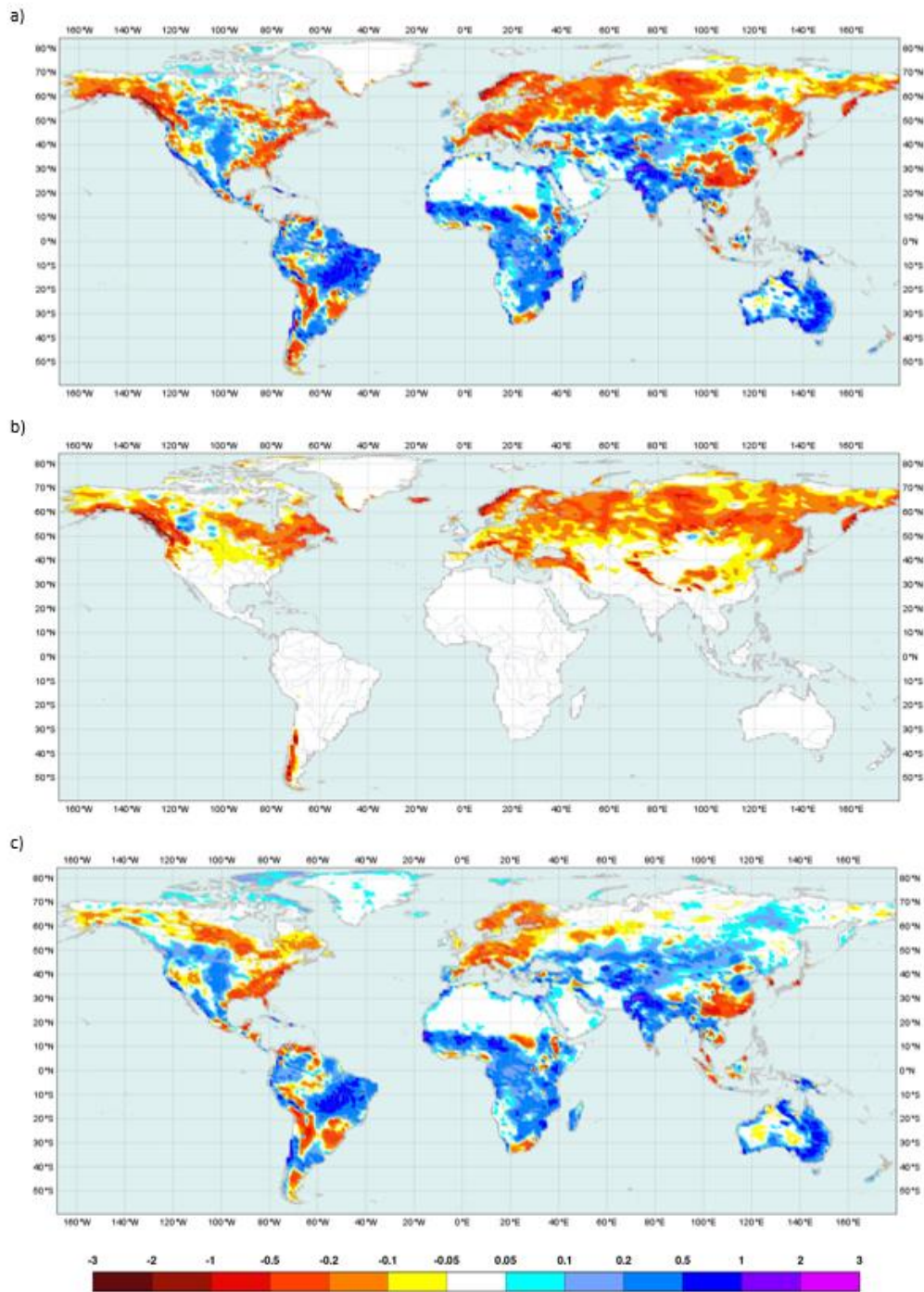
1077



1078

1079 Figure 4. Difference in the snow depth mean absolute errors between ONLINE and
 1080 OFFLINE for January based on observations in 2000-2007 (in cm). Points are shown where
 1081 observations are available. Blue colours indicate lower errors in the ONLINE experiment.

1082



1083

1084

Figure 5. Average daily water budget analysis (mm/day) of the ONLINE experiment based

1085

on the ERA5-D25 dataset for (a) the total 24-hour water budget errors, (b) the 24-hour snow

1086

water equivalent increments and (c) the 24-hour soil water content increments. Negative

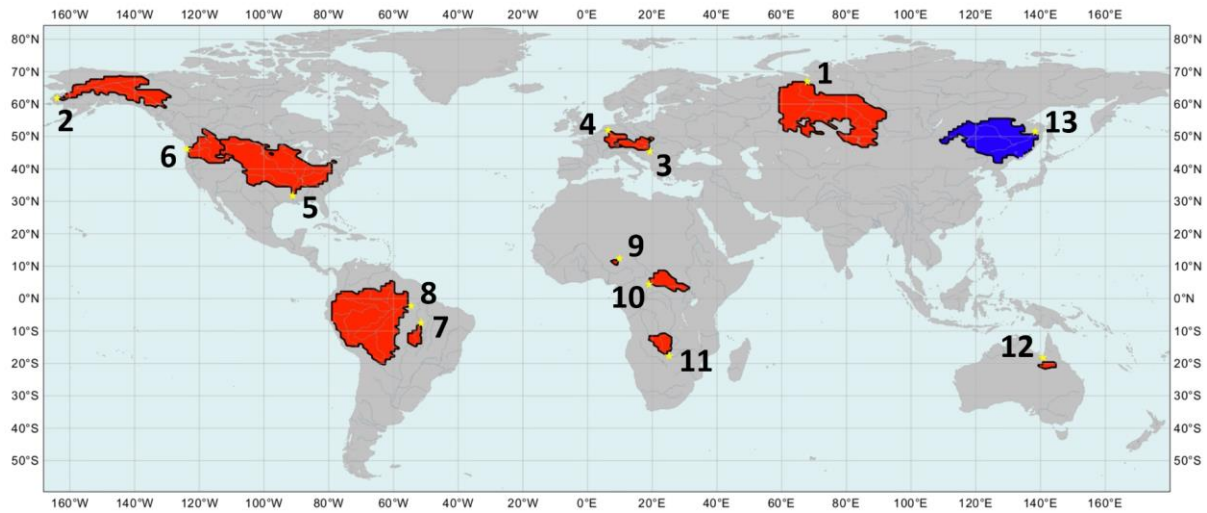
1087

values (red) indicate water removal by LDAS, while positive values (blue) show where water

1088

is added to the hydrological cycle.

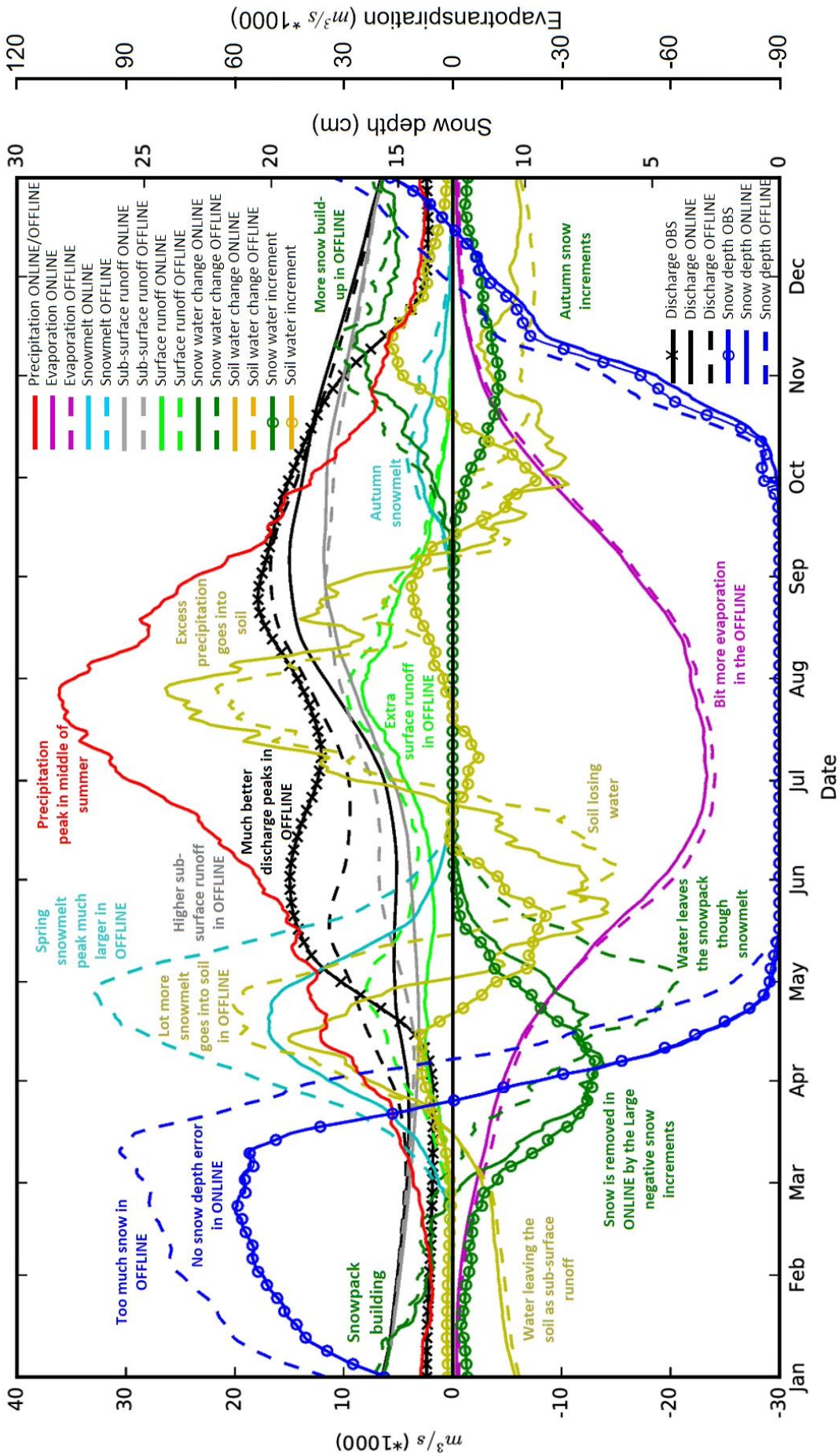
1089



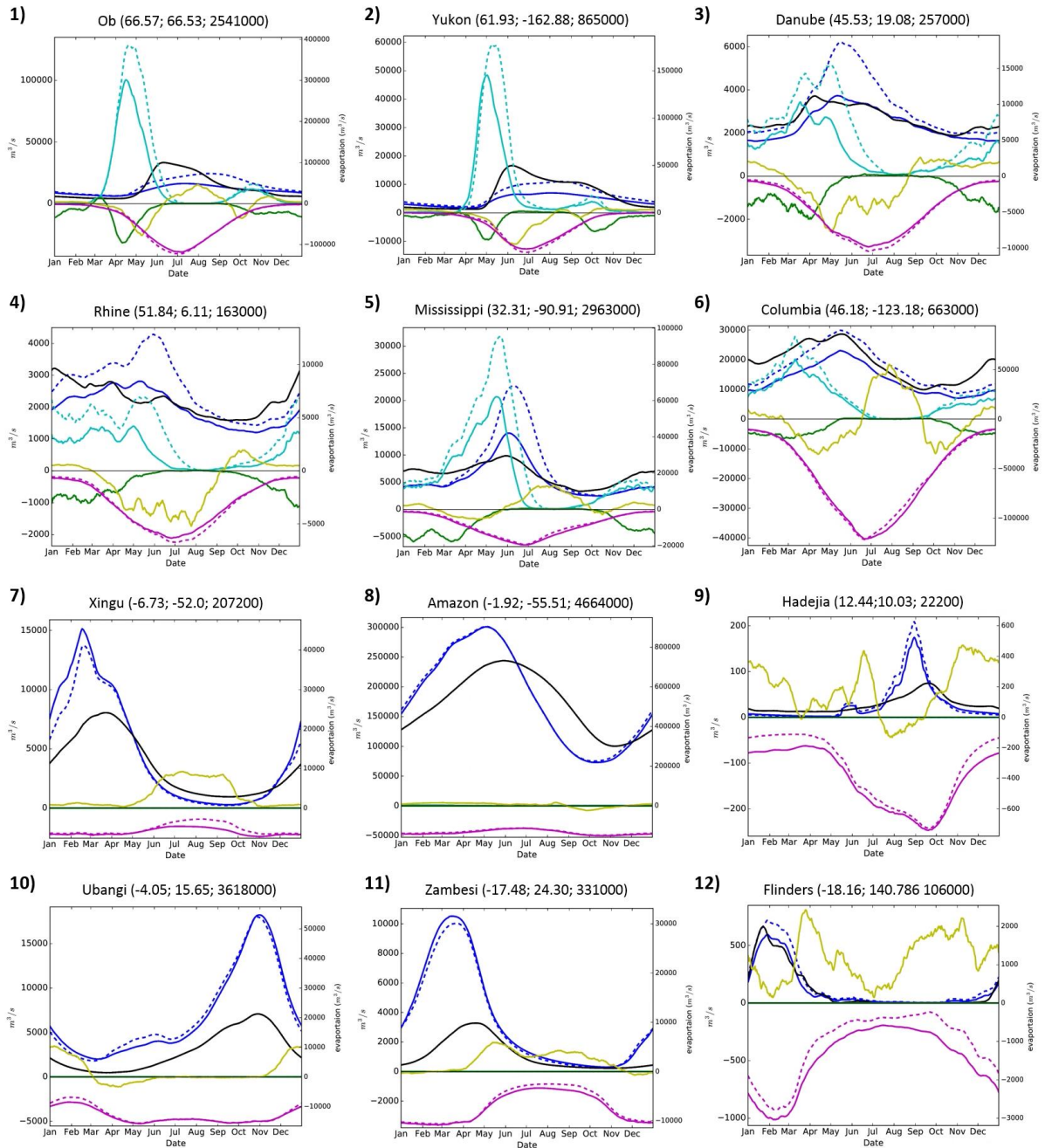
1090

1091 Figure 6. Map of the catchments analysed in Section 3.3 (Figure 7), where the catchment-
 1092 level process is examined over the Amur river (blue area, no. 13), and in Section 3.4 (Figure
 1093 8), where the simplified representation of the annual water cycle is shown for some selected
 1094 regional catchments of the world (red areas, no. 1-12). The catchment details are provided in
 1095 Table 3.

1096



1098 Figure 7. Average daily water budget cycle for a catchment on the Amur river in Russia at
1099 Komsomolsk. It includes the following parameters: precipitation (red line), snow (green line
1100 with markers) and soil (mustard line with markers) water content increments for the ONLINE
1101 simulation; surface runoff (light green), subsurface runoff (grey), evapotranspiration
1102 (magenta), snowmelt (cyan) and soil (mustard) and snow (green) water storage daily changes
1103 for both ONLINE (solid lines) and OFFLINE (dashed lines); snow depth (blue) and also river
1104 discharge (black) for the ONLINE (solid lines) and OFFLINE (dashed lines) experiments and
1105 also observations (lines with markers). The snow depth values are based on 2000-2007 while
1106 all other displayed daily climatological means are based on the ERA5-D25 dataset (for more
1107 detail on the computation of these values see Section 2.11 and 2.12).
1108



1109

1110 Figure 8. The annual cycle of water budget variables for a selection of catchments worldwide

1111 numbered from 1 to 12 (see Figure 6). The displayed variables are the snowmelt (cyan),

1112 evapotranspiration (magenta) and river discharge (blue) for both the ONLINE (solid lines)

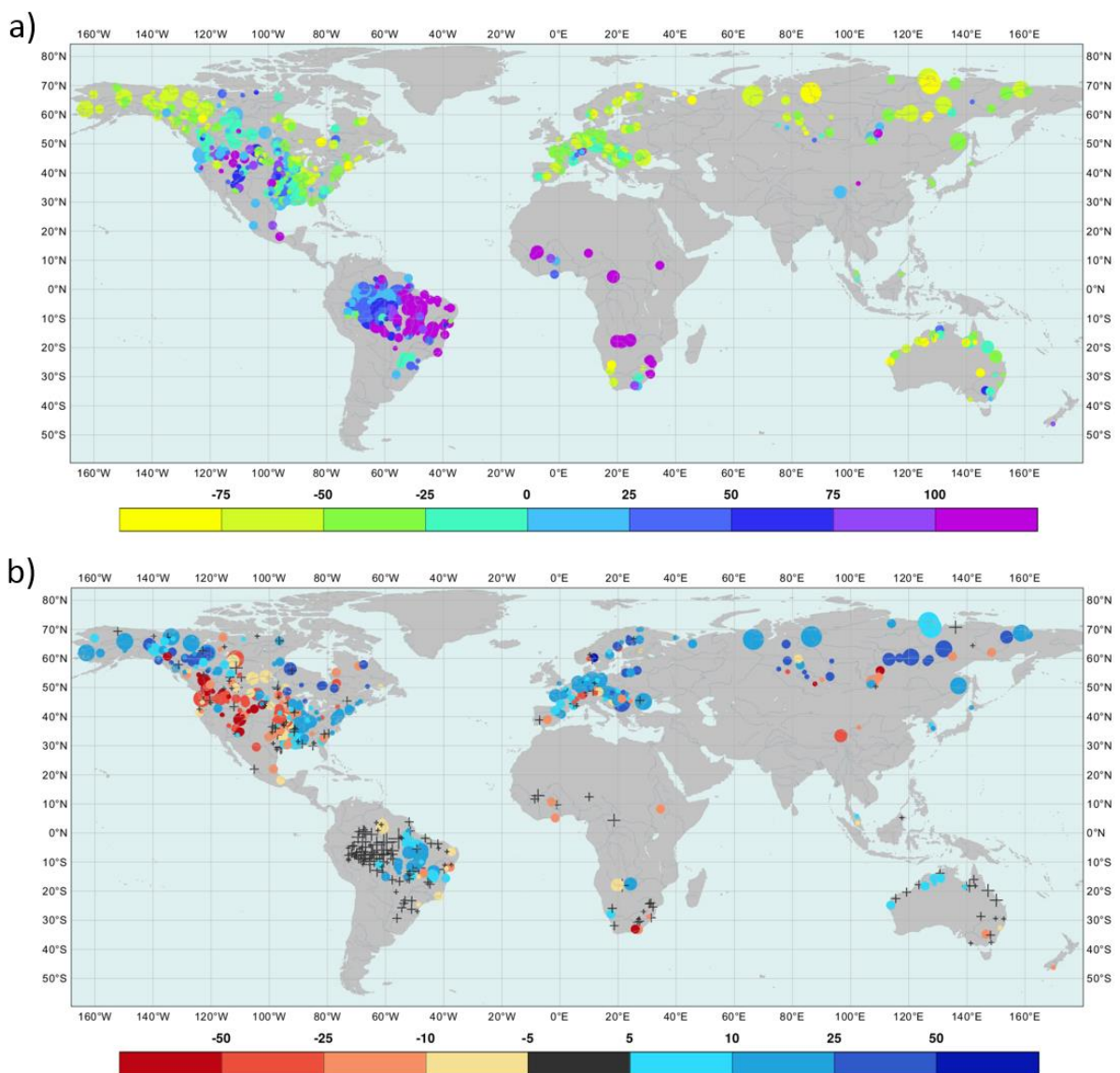
1113 and OFFLINE (dashed lines) experiments, the snow (green) and soil (mustard) increments for

1114 ONLINE and the river discharge observations (black line). All values are daily climatological

1115 averages based on the ERA5-D25 dataset (for details on the computation of these values see

1116 Section 2.12). The river names, the gauge coordinates and the upstream area values are

1117 displayed in the subplot titles. The catchment descriptions with the main verification score
1118 values for the ONLINE and OFFLINE simulations are provided in Table 3. In addition, the
1119 catchment area contours are provided in Figure 6. The evapotranspiration scale is provided on
1120 the secondary vertical axis while the scale for all other parameters is shown on the main
1121 vertical axis.
1122



1123
1124 Figure 9. River discharge percentage peak magnitude (a) ME (in %) of the ONLINE
1125 experiment and (b) change in the percentage peak magnitude MAE (in %) between ONLINE
1126 and OFFLINE based on the ERA5-D25 dataset. Positive error differences in b) indicate

1127 deterioration (blue) while negative changes show improvement (red) in the ONLINE
1128 simulation compared with OFFLINE. The catchments are displayed with different marker
1129 sizes representing the size of the catchment area. Near zero differences are shown by black
1130 crosses, while all other categories are displayed by circles.